ChemComm

COMMUNICATION

View Article Online
View Journal | View Issue

Cite this: *Chem. Commun.*, 2024, **60**, 8399

Received 27th May 2024,
Accepted 10th July 2024

DOI: 10.1039/d4cc02522a

rsc.li/chemcomm

Modulation of Fe–Fe distance and spin in diiron complexes using tetradentate ligands with different flanking donors†

Kyle D. Spielvogel,[a] Emily J. Campbell,[a] Sabyasachi Roy Chowdhury,[b] Florian Benner,[c] Selvan Demir,[c] Gillian P. Hatzis,[d] Hayley R. Petras,[a] Dunya Sembukuttiarachchige,[a] James J. Shepherd,[a] Christine M. Thomas,[d] Bess Vlaisavljevich[ab] and Scott R. Daly*[a]

Here we report the synthesis and characterization of diiron complexes containing triaryl N_4 and N_2S_2 ligands derived from *o*-phenylenediamine. The complexes display significant differences in Fe–Fe distances and magnetic properties that depend on the identity of the flanking NMe_2 and SMe donor groups.

Dinuclear iron complexes are renowned for their functional roles in metalloenzymes and biomimetic complexes.[1] They are also highly relevant to efforts aimed at understanding chemical factors that govern the strength of metal–metal interactions with first-row transition metals, especially when combined with weak field ligands.[2,3] These 3d complexes are often paramagnetic and adopt different spin configurations that depend sensitively on the degree of coupling between the metals. This has led to interest in understanding how ligand and structural modifications can be used to control spin states and associated magnetic properties for spin-based applications.[3,4]

Amido ligands have been featured prominently in efforts aimed at preparing dinuclear complexes with iron. Examples include $Fe_2[N(SiMe_3)_2]_4$ and related complexes that form a diamond Fe_2N_2 core in the solid state.[5–7] Other examples include amido ligands containing appended metal-donor groups.[8] These have been used most extensively to prepare diiron complexes that are C_3 symmetric with respect to the Fe–Fe axis,[9] but amido ligands derived from *o*-phenylenediamine have also been used to assemble iron complexes of various nuclearity. Betley and coworkers reported tripodal ligands containing three *o*-phenylenediamine units that can yield metal clusters containing up to six Fe atoms.[10,11] Similarly, a dinuclear Fe_2N_2 complex containing *N*,*N*′-bis(pentafluorophenyl)-*o*-phenylenediamide was recently described.[12]

We previously reported the triaryl N_4 and N_2S_2 ligands H_2(**L1**) and H_2(**L2**) (Fig. 1).[13,14] Like the examples described above, these tetradentate ligands are derived from *o*-phenylenediamine, but they contain flanking aryl groups with NMe_2 and SMe donor substituents. Here we report the synthesis and properties of homoleptic Fe(II) complexes with **L1** and **L2**. Unlike previous examples with Ni and Ru,[13,14] and prior studies of square-planar Fe(II) complexes with stronger field PNNP ligands,[15] the aryl groups and donor atoms in **L1** and **L2** do not remain conjugated and coordinated in the same plane. Instead, they give rise to dinuclear Fe complexes with structures and spin configurations that are highly dependent on the identity of the flanking NMe_2 and SMe donor groups.

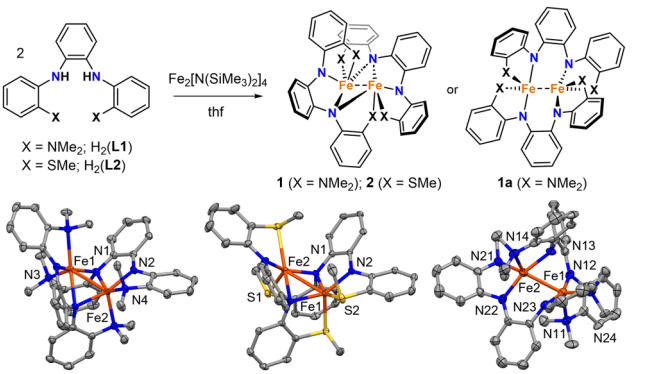

Fig. 1 Top: Synthesis of **1** (X = NMe_2) and **2** (X = SMe) and structural isomer observed with X = NMe_2 (**1a**). Bottom: Molecular structures of **1** (left), **2** (center), and **1a** (right). Thermal ellipsoids are drawn at the 50% level (data collected at 150 K). Hydrogen atoms and co-crystallized solvent were removed from the figure. Only one of the two crystallographically unique complexes in the unit cell of **1a** is shown.

[a] *The University of Iowa, Department of Chemistry, E331 Chemistry Building, Iowa City, IA 52242, USA. E-mail: scott-daly@uiowa.edu*
[b] *The University of South Dakota, Department of Chemistry, 414 E Clark St., Vermillion SD, 57069, USA*
[c] *Michigan State University, Department of Chemistry, 578 South Shaw Lane, East Lansing, Michigan 48824, USA*
[d] *The Ohio State University, Department of Chemistry and Biochemistry, 100 West 18th Ave, Columbus, OH 43210, USA*

† Electronic supplementary information (ESI) available: Experimental and computational details. CCDC 2357235–2357238. For ESI and crystallographic data in CIF or other electronic format see DOI: https://doi.org/10.1039/d4cc02522a

Mixing H_2(**L1**) or H_2(**L2**) with *in situ* generated $Fe_2[N(SiMe_3)_2]_4$ in thf resulted in dark red solutions, and subsequent workup and crystallization by vapor diffusion of pentane into concentrated benzene solutions yielded large dark red crystals of **1** and **2**. Both complexes were isolated as single crystals in good yields (67% and 85%, respectively).

The dinuclear structures of **1** and **2** were revealed by single-crystal X-ray diffraction studies. Each complex has a butterfly Fe_2N_2 core supported by bridging amido groups on separate ligands (Fig. 1). The most apparent difference between the two structures is the Fe–Fe distances of 2.5072(5) and 2.7666(6) Å for **1** and **2**, respectively (Fig. 2). The Fe–Fe distance in **1** is significantly shorter than those reported for amido-bridged complexes $Fe_2[N(SiMe_3)_2]_4$, $Fe_2[N(SiMe_3)_2]_2[OC(CF_3)_2Ph]_2$, and $Fe_2(NPh_2)_4$ at 2.663(2), 2.674(6), and 2.715(2) Å, respectively,[6] and is effectively identical to the 2.5128(4) Å distance very recently reported for $Fe_2(TMP)_2(C_6F_5)_2$ (TMP = tetramethylpiperidide).[7] The distance corresponds to a formal shortness ratio (FSR) of 1.08, which is just beyond the range expected for a formal Fe–Fe single bond.[3]

The close Fe–Fe distances are supported by bridging, but inequivalent, Fe–N bonds in the Fe_2N_2 core. Each bridging amido group forms a covalent N–Fe bond (X-type donor) with one Fe and a dative N → Fe bond (L-type donor) with the other, as indicated by the differing Fe–N distances (Fig. 2). The Fe–N bonds in **2** are 0.04 Å shorter on average compared to those in **1**.

Prior to assessing the magnetism of the complexes, unit cell checks were performed in addition to elemental analysis to confirm the purity of crystals obtained for different batches. It was during these checks that we discovered a second structural isomer of **1** in one of the batches prepared in the latter part of our investigation. To distinguish between the two structures, we will refer to the second isomer as **1a** (Fig. 1). Crystals of both isomers were grown by vapor diffusion of pentane into benzene solutions of **1**. Crystals of **1** with the intact Fe_2N_2 diamond core crystallize as relatively large blocks in the monoclinic space group $P2_1/c$ with 1.5 equivalents of co-crystallized benzene, whereas **1a** crystallizes as small irregular prisms in the triclinic space group $P\bar{1}$ and has an equivalent of co-crystallized benzene and disordered solvent presumed to be pentane. The biggest change in the structure of **1a** with respect to **1** is the opening of the Fe_2N_2 core. The L-type bonds associated with the amido bridges in **1** are no longer present in **1a**. As a result, the Fe–Fe distance in **1** at 2.5072(5) Å elongates to 2.627(2) Å in **1a**, and the X-type Fe–N bonds shorten by 0.05–0.08 Å. A second polymorph of **2** containing co-crystallized benzene was also discovered (**2a**), but unlike **1** and **1a**, there were only subtle differences in their structures (Fig. S1, ESI†).

Magnetometry studies were performed to investigate the magnetic properties of **1** and **2**. Given the possibility of two isomers for **1**, we investigated the room temperature magnetic moments first in solution and then in the solid state on crystallographically authenticated samples of both complexes. Evans method magnetic measurements performed on benzene solutions of **1** and **2** revealed effective magnetic moments of 7.6 and 6.3 μ_B, respectively. Solid-state measurements made using a magnetic susceptibility balance at room temperature (294 K) yielded effectively identical magnetic moments of 7.6(1) μ_B for **1** and 6.2(1) μ_B for **2**. This suggests that the differences in μ_{eff} for **1** and **2** cannot be attributed to phase-dependent differences in structure or crystal packing. It may also suggest that the structure of **1** persists in solution or that the structure of **1a** has little influence on the magnetic moment.

Dc magnetic susceptibility data were collected on polycrystalline samples of **1** and **2** using a SQUID magnetometer field of 1.0 T to measure the temperature dependence of the molar magnetic susceptibility times temperature ($\chi_M T$ *vs.* T) for each sample (Fig. 3). The room temperature effective magnetic moments of 7.43 μ_B (**1**) and 6.02 μ_B (**2**) are in excellent agreement with the moments determined *via* Evans method and susceptibility balance (Fig. S2–S5, ESI†). For **1**, the room temperature $\chi_M T$ value of 6.900 cm^3 K mol^{-1} remains largely unchanged when lowering the temperature to ∼110 K, below which a gradual decrease in $\chi_M T$ value of 5.002 cm^3 K mol^{-1} is monitored (Fig. 3). Below ∼10 K a steep drop in $\chi_M T$ is observed, which is largely attributed to zero-field splitting and/or antiferromagnetic coupling. The magnetic data was modeled under consideration of a weak antiferromagnetic coupling interaction between the two Fe(II) centers with a J of −0.22(3) cm^{-1} (Table S2, ESI†). For **2**, exhibiting the longer

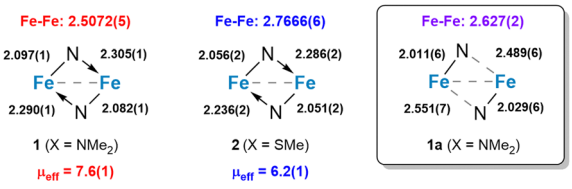

Fig. 2 Summary of distances (Å) in the Fe_2N_2 core in **1**, **2**, and **1a** and comparison to the RT μ_{eff} values in μ_B (susceptibility balance). Distances for **1a** are shown for one of two crystallographically unique complexes in the asymmetric unit cell, but they are representative of both complexes.

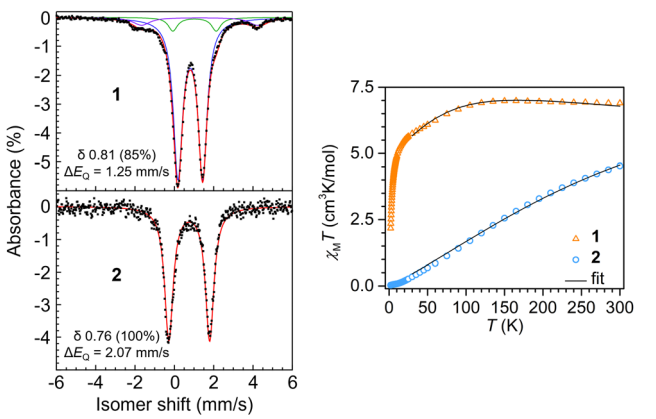

Fig. 3 Left: ^{57}Fe Mössbauer spectra of **1** and **2** at 4 K. Right: Variable-temperature (zero-field-cooled (zfc)) dc magnetic susceptibility data for restrained polycrystalline samples of **1** and **2** collected under a 1.0 T applied dc field. The black lines represent fits to the data from 30 to 300 K for **1** and **2**, respectively.

Fe–Fe distance, the trend in progression of the dc magnetic susceptibility data from **2** to 300 K varies significantly relative to **1**. The room temperature $\chi_M T$ value is 4.528 cm^3 K mol^{-1}, which declines almost linearly with decreasing temperatures, resulting in a $\chi_M T$ value of 0.030 cm^3 K mol^{-1} at 2 K, which is close to zero. Such static magnetic susceptibility behavior is indicative of strong antiferromagnetic coupling and hence, was modeled accordingly, yielding a J value of $-37(1)$ cm^{-1}. This magnitude of J represents a 168-fold increase in magnetic coupling for **2** compared to **1** despite the longer Fe–Fe distance in **2** (Table S3, ESI†).

^{57}Fe Mössbauer spectra were collected on **1** and **2** to evaluate Fe oxidation states and electronic environment. The spectrum of **1** at 20 K revealed two quadrupole doublets (Fig. S6, ESI†). The major component (83%) had an isomer shift of δ 0.80 (ΔE_Q = 1.25 mm s^{-1}), consistent with high-spin Fe(II). A minor component was observed at a nearly identical isomer shift of δ 0.84, but it displayed a larger quadrupole splitting (2.43 mm s^{-1}). Cooling the sample further to 4 K yielded no effective change in the major component (δ 0.81; 1.25 mm s^{-1}; 85%), but the minor component appears to undergo additional hyperfine splitting (Fig. 3). As with our magnetic measurements, random unit cell checks of the crystal batch used for Mössbauer analysis were uniformly consistent with **1**, but it is possible that the minor component could be attributed to small amounts of co-crystallized **1a**. We think it is more likely that the minor component is attributed to a non-integer spin impurity, which would be consistent with the additional hyperfine splitting observed upon sample cooling.

The Mössbauer spectrum of **2** at 4 K revealed a quadrupole doublet that was modeled as a single high-spin Fe(II) species. The isomer shift of δ 0.76 is similar to the δ 0.81 shift for **1**, but the spectrum for **2** displays a larger quadrupole splitting of 2.07 mm s^{-1}. This increase is consistent with the reduction in spin due to the increased antiferromagnetic coupling. For example, Betley and coworkers showed that a reduction in S = 4 to S = 2 in *o*-phenylenediamido-supported triiron clusters capped with ancillary pyridine ligands at 105 K led to an increase in quadrupolar splitting from ΔE_Q = 1.48 mm s^{-1} to ΔE_Q = 2.22 mm s^{-1},[11] but with nearly identical isomer shifts of δ 0.85 and 0.82, respectively, as observed for **1** and **2**.

DFT calculations (B3LYP-D3/def2-TZVP)[16] were performed to evaluate the energies and structural preferences of **1** with respect to **1a**. All attempts to optimize **1** resulted in geometries with bond distances consistent with **1a**, indicating that this species lies lower in energy (Tables S4–S6, ESI†). The DFT calculated Fe–Fe distance for **1a** was 2.687 Å, only a 0.060 Å (2.3%) deviation from experiment. To calculate the structure of **1**, the Fe atoms were fixed at their experimental positions while the remaining ligand atoms were allowed to relax. This fixed species, which is denoted herein as **1′**, is nearly 3 kcal mol^{-1} higher in energy than **1a** according to DFT (Tables S5 and S6, ESI†). Likewise, CASPT2[17] calculations yielded a consistent energy difference of 5.6 kcal mol^{-1} (Table S5, ESI†). These relatively small energy differences agree with our ability to isolate both structures.

Geometry optimizations of **2** also yielded a structure in excellent agreement with experiment (Fe–Fe distance of 2.807 Å; 0.040 Å (1.5%) deviation from XRD), as shown with overlays of the computed and experimental structures (Fig. S10, ESI†). Although DFT optimizations were performed only for the S = 4 DFT ground state (Tables S7 and S8, ESI†), CASPT2 calculations revealed that the lowest energy spin configuration for **1′**, **1a**, and **2** was S = 0 (Table S9, ESI†). However, the other spin states (S = 1, 2, 3, and 4) were all within 1.2 kcal mol^{-1}, which falls within the error of the CASPT2 method. This indicates that the assignment of the ground spin state would require careful treatment of both spin–orbit coupling and electron correlation. The observation of closely spaced spin multiplets is consistent with no interaction between the Fe centers, as can be seen in the CASSCF natural orbitals (Fig. S8, ESI†). On the other hand, some orbital overlap is present in DFT (Fig. S9, ESI†), resulting in a Mayer bond-order between the metal ions of 0.1 for **1′** and **1a** and 0.05 for **2** (Table S10, ESI†). These differing observations are consistent with the more localized bonding in the CASSCF natural orbitals, which suggest no Fe–Fe bonding, compared to the DFT Kohn–Sham orbitals, which suggest the existence of very weak Fe–Fe bonding.

In summary, we have described how triaryl tetradentate ligands derived from *o*-phenylenediamine form diiron complexes that have Fe–Fe distances and magnetic properties that are highly sensitive to the identity of the flanking donor substituents. These results compliment studies showing how ancillary ligand field strength can significantly alter Fe–Fe distances and spin states in triiron complexes supported by hexadentate ligands derived from *o*-phenylenediamine.[11] Rather than using ancillary ligands, we have shown here that exchanging flanking donors can be used to achieve similar outcomes. In addition to our ongoing studies with iron, we are currently investigating these dinucleating ligand effects with other first-row transition metals. These efforts will be described in several upcoming reports.

KDS, DS, and SRD thank the NSF for support (CHE-1650894), and Dale Swenson for collecting the XRD data. The structure of **1a** was collected using the instrument supported by NSF CHE-1828117. JJS, HRP, and EJC thank the University of Iowa for support. GPH and CMT acknowledge the NSF for support (CHE-2101002). SD and FB also thank the NSF for support through the CAREER award to SD (CHE-2339595). SRC and BV thank the U.S. DOE, Office of Science, BES, Computational Chemical Sciences program for support under award number DE-SC0019463. Computations supporting this project performed on high-performance computing systems were made possible by resources funded by NSF award OAC-1626516.

Data availability

Input and output files associated with all calculations are available both in a FigShare repository (**https://doi.org/10.6084/m9.figshare.26121724**) and in an ioChem-BD repository (**https://doi.org/10.19061/iochem-bd-6-379**). Crystallographic data has been deposited at the CCDC under 2357235–2357238. The remaining data have been included as part of the ESI.†

Conflicts of interest

There are no conflicts to declare.

Notes and references

1 (*a*) A. J. Jasniewski and L. Que, Jr., *Chem. Rev.*, 2018, **118**, 2554–2592; (*b*) Y. Li and T. B. Rauchfuss, *Chem. Rev.*, 2016, **116**, 7043–7077; (*c*) T. B. Rauchfuss, *Acc. Chem. Res.*, 2015, **48**, 2107–2116; (*d*) P. A. Lindahl, *J. Inorg. Biochem.*, 2012, **106**, 172–178; (*e*) L. H. Do and S. J. Lippard, *J. Inorg. Biochem.*, 2011, **105**, 1774–1785; (*f*) S. Friedle, E. Reisner and S. J. Lippard, *Chem. Soc. Rev.*, 2010, **39**, 2768–2779.

2 (*a*) R. J. Eisenhart, L. J. Clouston and C. C. Lu, *Acc. Chem. Res.*, 2015, **48**, 2885–2894; (*b*) R. H. Duncan Lyngdoh, H. F. Schaefer, III and R. B. King, *Chem. Rev.*, 2018, **118**, 11626–11706.

3 J. A. Chipman and J. F. Berry, *Chem. Rev.*, 2020, **120**, 2409–2447.

4 H. Oshio and M. Nihei, *Bull. Chem. Soc. Jpn.*, 2007, **80**, 608–620.

5 (*a*) R. A. Andersen, K. Faegri, Jr., J. C. Green, A. Haaland, M. F. Lappert, W. P. Leung and K. Rypdal, *Inorg. Chem.*, 1988, **27**, 1782–1786; (*b*) S. Takemoto, S.-I. Ogura, H. Yo, Y. Hosokoshi, K. Kamikawa and H. Matsuzaka, *Inorg. Chem.*, 2006, **45**, 4871–4873; (*c*) R. A. Lewis, S. Morochnik, A. Chapovetsky, G. Wu and T. W. Hayton, *Angew. Chem., Int. Ed.*, 2012, **51**, 12772–12775; (*d*) T. Deschner, K. W. Törnroos and R. Anwander, *Inorg. Chem.*, 2011, **50**, 7217–7228; (*e*) L. M. Aguirre Quintana, Y. Yang, A. Ramanathan, N. Jiang, J. Bacsa, L. Maron and H. S. La Pierre, *Chem. Commun.*, 2021, **57**, 6664–6667; (*f*) R. Köster, G. Seidel, R. Boese and B. Wrackmeyer, *Chem. Ber.*, 1987, **120**, 669–683; (*g*) T. Hatakeyama, R. Imayoshi, Y. Yoshimoto, S. K. Ghorai, M. Jin, H. Takaya, K. Norisuye, Y. Sohrin and M. Nakamura, *J. Am. Chem. Soc.*, 2012, **134**, 20262–20265; (*h*) C. Ni, G. J. Long, F. Grandjean and P. P. Power, *Inorg. Chem.*, 2009, **48**, 11594–11600; (*i*) S. Ohta, Y. Ohki, Y. Ikagawa, R. Suizu and K. Tatsumi, *J. Organomet. Chem.*, 2007, **692**, 4792–4799.

6 (*a*) M. M. Olmstead, P. P. Power and S. C. Shoner, *Inorg. Chem.*, 1991, **30**, 2547–2551; (*b*) M. A. Chacon-Teran, S. E. Creutz, R. E. Rodriguez-Lugo, S. Demeshko, F. Meyer, A. Kajetanowicz and K. Grela, *Organometallics*, 2024, **43**, 564–572.

7 A. Logallo, L. C. H. Maddock, M. Mu, L. Gravogl, N. Jin, M. N. Peñas-Defrutos, K. Meyer, M. García-Melchor and E. Hevia, *Angew. Chem., Int. Ed.*, 2024, e202402907.

8 (*a*) A. J. Elias, H. W. Roesky, W. T. Robinson and G. M. Sheldrick, *J. Chem. Soc., Dalton Trans.*, 1993, 495–500; (*b*) J. Chai, H. Zhu, Q. Ma, Roesky, W. Herbert, H.-G. Schmidt and M. Noltemeyer, *Eur. J. Inorg. Chem.*, 2004, 4807–4811; (*c*) C. Koch, A. Malassa, C. Agthe, H. Görls, R. Biedermann, H. Krautscheid and M. Westerhausen, *Z. Anorg. Allg. Chem.*, 2007, **633**, 375–382; (*d*) A. K. Das, Z. Moatazedi, G. Mund, A. J. Bennet, R. J. Batchelor and D. B. Leznoff, *Inorg. Chem.*, 2007, **46**, 366–368; (*e*) A. Malassa, N. Herzer, H. Görls and M. Westerhausen, *Dalton Trans.*, 2010, **39**, 5356–5366.

9 (*a*) J. P. Krogman and C. M. Thomas, *Chem. Commun.*, 2014, **50**, 5115–5127; (*b*) F. A. Cotton, L. M. Daniels, L. R. Falvello and C. A. Murillo, *Inorg. Chim. Acta*, 1994, **219**, 7–10; (*c*) F. A. Cotton, L. M. Daniels, L. R. Falvello, J. H. Matonic and C. A. Murillo, *Inorg. Chim. Acta*, 1997, **256**, 269–275; (*d*) C. M. Zall, D. Zherebetskyy, A. L. Dzubak, E. Bill, L. Gagliardi and C. C. Lu, *Inorg. Chem.*, 2012, **51**, 728–736; (*e*) S. Kuppuswamy, T. M. Powers, B. M. Johnson, M. W. Bezpalko, C. K. Brozek, B. M. Foxman, L. A. Berben and C. M. Thomas, *Inorg. Chem.*, 2013, **52**, 4802–4811; (*f*) S. Kuppuswamy, T. M. Powers, J. P. Krogman, M. W. Bezpalko, B. M. Foxman and C. M. Thomas, *Chem. Sci.*, 2013, **4**, 3557–3565; (*g*) S. Kuppuswamy, M. W. Bezpalko, T. M. Powers, M. J. T. Wilding, C. K. Brozek, B. M. Foxman and C. M. Thomas, *Chem. Sci.*, 2014, **5**, 1617–1626; (*h*) B. Wu, M. J. T. Wilding, S. Kuppuswamy, M. W. Bezpalko, B. M. Foxman and C. M. Thomas, *Inorg. Chem.*, 2016, **55**, 12137–12148; (*i*) S. M. Greer, J. McKay, K. M. Gramigna, C. M. Thomas, S. A. Stoian and S. Hill, *Inorg. Chem.*, 2018, **57**, 5870–5878; (*j*) B. A. Barden, G. Culcu, J. P. Krogman, M. W. Bezpalko, G. P. Hatzis, D. A. Dickie, B. M. Foxman and C. M. Thomas, *Inorg. Chem.*, 2019, **58**, 821–833; (*k*) S. M. Greer, K. M. Gramigna, C. M. Thomas, S. A. Stoian and S. Hill, *Inorg. Chem.*, 2020, **59**, 18141–18155; (*l*) L. J. Clouston, R. B. Siedschlag, P. A. Rudd, N. Planas, S. Hu, A. D. Miller, L. Gagliardi and C. C. Lu, *J. Am. Chem. Soc.*, 2013, **135**, 13142–13148; (*m*) C. M. Zall, L. J. Clouston, V. G. Young, Jr., K. Ding, H. J. Kim, D. Zherebetskyy, Y.-S. Chen, E. Bill, L. Gagliardi and C. C. Lu, *Inorg. Chem.*, 2013, **52**, 9216–9228; (*n*) S. J. Tereniak, R. K. Carlson, L. J. Clouston, V. G. Young, E. Bill, R. Maurice, Y.-S. Chen, H. J. Kim, L. Gagliardi and C. C. Lu, *J. Am. Chem. Soc.*, 2014, **136**, 1842–1855; (*o*) R. C. Cammarota and C. C. Lu, *J. Am. Chem. Soc.*, 2015, **137**, 12486–12489; (*p*) L. J. Clouston, V. Bernales, R. C. Cammarota, R. K. Carlson, E. Bill, L. Gagliardi and C. C. Lu, *Inorg. Chem.*, 2015, **54**, 11669–11679; (*q*) R. J. Eisenhart, P. A. Rudd, N. Planas, D. W. Boyce, R. K. Carlson, W. B. Tolman, E. Bill, L. Gagliardi and C. C. Lu, *Inorg. Chem.*, 2015, **54**, 7579–7592; (*r*) D. L. Miller, R. B. Siedschlag, L. J. Clouston, V. G. Young, Y.-S. Chen, E. Bill, L. Gagliardi and C. C. Lu, *Inorg. Chem.*, 2016, **55**, 9725–9735; (*s*) J. T. Moore, S. Chatterjee, M. Tarrago, L. J. Clouston, S. Sproules, E. Bill, V. Bernales, L. Gagliardi, S. Ye, K. M. Lancaster and C. C. Lu, *Inorg. Chem.*, 2019, **58**, 6199–6214; (*t*) J. R. Prat, C. A. Gaggioli, R. C. Cammarota, E. Bill, L. Gagliardi and C. C. Lu, *Inorg. Chem.*, 2020, **59**, 14251–14262; (*u*) R. C. Cammarota, L. J. Clouston and C. C. Lu, *Coord. Chem. Rev.*, 2017, **334**, 100–111; (*v*) A. Z. Spentzos, S. R. May, A. M. Confer, M. R. Gau, P. J. Carroll, D. P. Goldberg and N. C. Tomson, *Inorg. Chem.*, 2023, **62**, 11487–11499.

10 (*a*) T. D. Harris and T. A. Betley, *J. Am. Chem. Soc.*, 2011, **133**, 13852–13855; (*b*) T. D. Harris, Q. Zhao, R. Hernandez Sanchez and T. A. Betley, *Chem. Commun.*, 2011, **47**, 6344–6346; (*c*) T. M. Powers, A. R. Fout, S.-L. Zheng and T. A. Betley, *J. Am. Chem. Soc.*, 2011, **133**, 3336–3338; (*d*) Q. Zhao and T. A. Betley, *Angew. Chem., Int. Ed.*, 2011, **50**, 709–712; (*e*) Q. Zhao, T. D. Harris and T. A. Betley, *J. Am. Chem. Soc.*, 2011, **133**, 8293–8306; (*f*) E. V. Eames and T. A. Betley, *Inorg. Chem.*, 2012, **51**, 10274–10278; (*g*) E. V. Eames, R. Hernandez Sanchez and T. A. Betley, *Inorg. Chem.*, 2013, **52**, 5006–5012; (*h*) T. M. Powers and T. A. Betley, *J. Am. Chem. Soc.*, 2013, **135**, 12289–12296; (*i*) T. M. Powers, N. X. Gu, A. R. Fout, A. M. Baldwin, R. Hernandez Sanchez, D. M. Alfonso, Y.-S. Chen, S.-L. Zheng and T. A. Betley, *J. Am. Chem. Soc.*, 2013, **135**, 14448–14458; (*j*) R. Hernandez Sanchez and T. A. Betley, *J. Am. Chem. Soc.*, 2015, **137**, 13949–13956; (*k*) R. Hernandez Sanchez, A. M. Willis, S.-L. Zheng and T. A. Betley, *Angew. Chem., Int. Ed.*, 2015, **54**, 12009–12013; (*l*) R. Hernandez Sanchez, A. K. Bartholomew, T. M. Powers, G. Menard and T. A. Betley, *J. Am. Chem. Soc.*, 2016, **138**, 2235–2243; (*m*) R. Hernandez Sanchez and T. A. Betley, *J. Am. Chem. Soc.*, 2018, **140**, 16792–16806.

11 E. V. Eames, T. D. Harris and T. A. Betley, *Chem. Sci.*, 2012, **3**, 407–415.

12 A. Hernán-Gómez, M. Rodríguez, T. Parella and M. Costas, *Angew. Chem., Int. Ed.*, 2019, **58**, 13904–13911.

13 (*a*) K. D. Spielvogel, N. C. Stumme, T. V. Fetrow, L. Wang, J. A. Luna, J. M. Keith, S. K. Shaw and S. R. Daly, *Inorg. Chem.*, 2022, **61**, 2391–2401; (*b*) K. D. Spielvogel, J. A. Luna, S. M. Loria, L. P. Weisburn, N. C. Stumme, M. R. Ringenberg, G. Durgaprasad, J. M. Keith, S. K. Shaw and S. R. Daly, *Inorg. Chem.*, 2020, **59**, 10845–10853; (*c*) G. Durgaprasad, J. A. Luna, K. D. Spielvogel, C. Haas, S. K. Shaw and S. R. Daly, *Organometallics*, 2017, **36**, 4020–4031.

14 K. D. Spielvogel, E. J. Coughlin, H. Petras, J. A. Luna, A. Benson, C. M. Donahue, A. Kibasa, K. Lee, R. Salacinski, S. C. Bart, S. K. Shaw, J. J. Shepherd and S. R. Daly, *Inorg. Chem.*, 2019, **58**, 12756–12774.

15 (*a*) G. P. Hatzis and C. M. Thomas, *Chem. Commun.*, 2020, **56**, 8611–8614; (*b*) K. Lee and C. M. Thomas, *Inorg. Chem.*, 2021, **60**, 17348–17356; (*c*) J. E. Stevens, C. E. Moore and C. M. Thomas, *J. Am. Chem. Soc.*, 2023, **145**, 794–799.

16 (*a*) A. D. Becke, *J. Chem. Phys.*, 1996, **104**, 1040–1046; (*b*) A. D. Becke, *J. Chem. Phys.*, 1997, **107**, 8554–8560; (*c*) C. Lee, W. Yang and R. G. Parr, *Phys. Rev. B: Condens. Matter Mater. Phys.*, 1988, **37**, 785–789; (*d*) F. Weigend and R. Ahlrichs, *Phys. Chem. Chem. Phys.*, 2005, **7**, 3297–3305; (*e*) E. Caldeweyher, C. Bannwarth and S. Grimme, *J. Chem. Phys.*, 2017, **147**, 034112.

17 (*a*) K. Andersson, P. Å. Malmqvist and B. O. Roos, *J. Chem. Phys.*, 1992, **96**, 1218–1226; (*b*) K. Andersson, P. A. Malmqvist, B. O. Roos, A. J. Sadlej and K. Wolinski, *J. Phys. Chem.*, 1990, **94**, 5483–5488.

